Imaging in Proton Therapy

I. CT, DECT, and Multi Energy CT for Planning and Dose Calculations

By Hugo Bouchard, PhD, MCCPM

Associate Professor – Department of Physics – Université de Montréal

Principal Researcher – Imaging and Engineering Axis – CRCHUM

Medical Physicist – Department of Radiation Oncology – CHUM

Self Assessment Module (SAM)

AAPM-COMP meeting – 12 July 2020

CRCHUM

Université de Montréal

Objectives of this talk

At the end of this talk, you will be able to

1. Define the need for CT during proton beam treatment planning
2. Summarize the principles of CT and the role of X-ray energy on data
3. Summarize various CT technologies for resolving energy
4. Explain the principles of CT calibration for radiotherapy
5. Summarize the principles for extracting key radiotherapy quantities from CT

1. CT during proton treatment planning

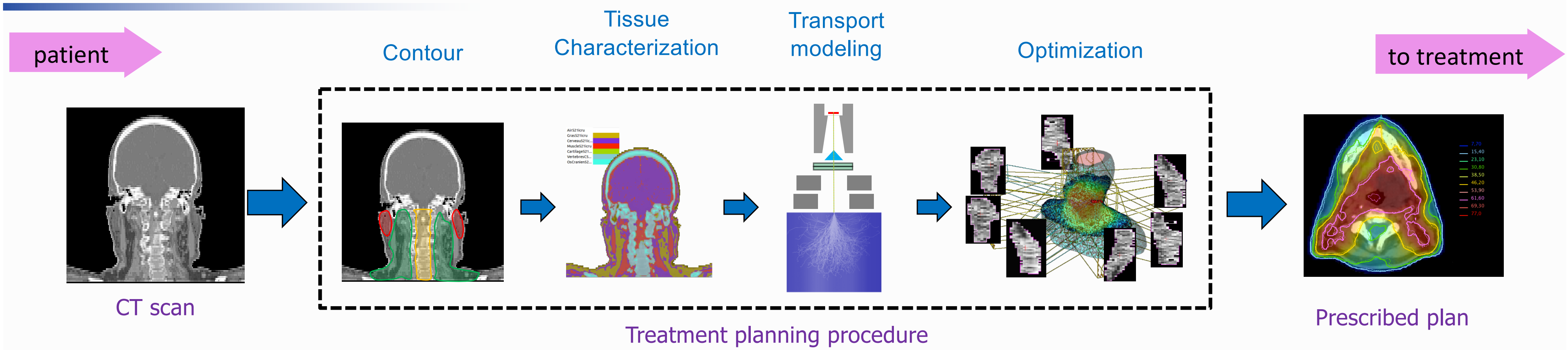

Roles of CT in radiotherapy treatment planning

1. Positioning : to provide an accurate representation of the patient geometry at the time of planning
2. Identification: to display image contrast provided by local variations of density and elemental composition
3. Quantification: to enable the conversion of CT numbers into radiotherapy quantities that are necessary for treatment planning

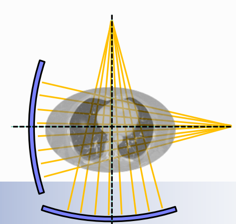

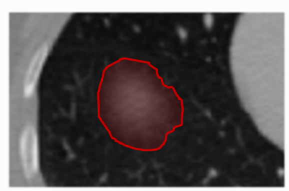

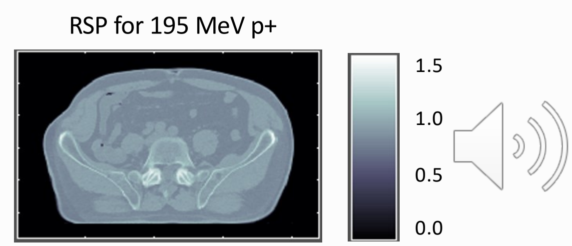

1. CT during proton treatment planning

Patient CT scan

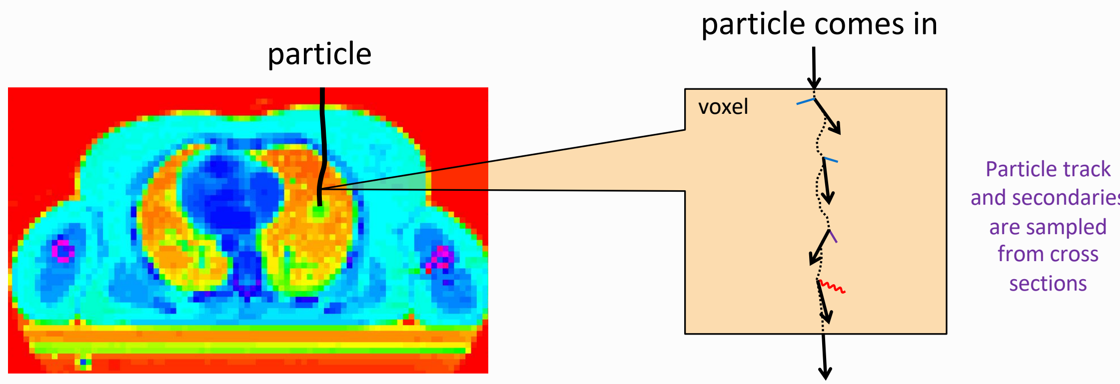

Voxelized geometry

particle comes out

- Proton range uncertainties can be reduced by more than 2% with Monte Carlo calculations compared to conventional methods (Paganetti, PMB 2012)
  - This is mostly due to the ability of MC to model range degradation
- Monte Carlo requires key input quantities to model interactions in human tissues
  - Macroscopic interaction cross sections
  - Stopping power

- There are at least 10 different physical processes relevant to radiotherapy (i.e., requiring the use of cross sections)
- Cross sections are energy- and *Z*-dependent and (mostly) unseparable functions
- Therefore dimensionality is governed by elemental composition

Interaction	Incident particle	Target	Z-dependance of $\sigma_a(E,Z)$
Rayleigh scattering	γ	atom	$F(Z)$
Photo-electric effect	γ	atom	$\sigma_{ph}(Z) \sim Z^5$
Compton scattering	γ	bound electrons	$S(Z)$
Pair and triplet production	γ	nucleus	$\sim Z(Z+\xi(Z))G_1(Z)$ and $Z(Z+\xi(Z))G_2(Z)$
Bremsstrahlung	e-, p+	nucleus	same as above
Collision stopping power	e-, p+	bound electrons	$\sim Z$ and $Z \ln I$
Coulomb scattering	e-, p+	nucleus	$Z^2 R(Z)$
EM collision (ionisation)	e-, p+	bound electrons	$\sim Z$ (except for EII)
Nuclear	p+	nucleus	isotope-specific
Atomic relaxation	all	atom	element-specific

1. CT during proton treatment planning

Macroscopic cross sections **Σ** are required to sample the distance between discrete interactions. They are linear combination of elemental atomic cross sections

$$\Sigma = \rho \sum_i w_i \frac{N_A}{A_i} \sigma_a (E, Z_i)$$

$\boldsymbol{\rho}$: mass density of medium (g/cm^3)
$\boldsymbol{\sigma}_a(E, Z_i)$: atomic cross section of i^{th} element (cm^2)
N_A : Avogadro's constant (mol^{-1})
A_i : molar mass of i^{th} element (g/mol)
w_i : elemental weight of i^{th} element

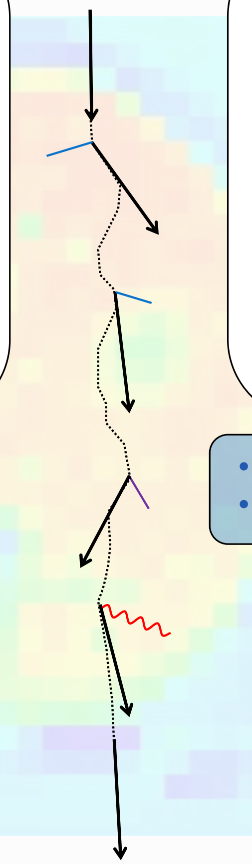

Collision stopping power is required to determine the energy loss between steps.

$$S_\Delta (T) = \rho \frac{Z}{A} N_A \frac{2\pi r_e^2 m_e c^2}{\beta^2} \left[\ln\left(\frac{2 m_e c^2 \gamma^2 \beta^2 T_{\text{up}}}{I^2} \right) - \beta^2 \left(1 + \frac{T_{\text{up}}}{T_{\max}} \right) - \delta - \frac{2C_e}{Z} + F \right]$$

I: mean excitation energy of medium (eV)
$\boldsymbol{\Delta}$: energy transfer cutoff (MeV)
δ : density effect correction
C_e: shell correction
F : higher-order corrections

$$T_{\max} = \frac{2 m_e c^2 (\gamma^2 - 1)}{1 + 2\gamma \left(\frac{m_e}{m_p} \right) + \left(\frac{m_e}{m_p} \right)^2} \qquad T_{\text{up}} = \min(\Delta, T_{\max})$$

Condensed history use MS theory to sample a combined deflection angle per step

$$p(\theta, \Omega) \approx k e^{-\frac{1}{2} \left[\frac{\theta}{\frac{13.6\ \text{MeV}}{\beta p c} \sqrt{\frac{l}{X_0}} \left[1 + 0{,}038 \ln\left(\frac{l}{X_0} \right) \right]} \right]^2}$$

X_0: radiation length being a function of $\boldsymbol{\rho} Z^2/A$

- Elemental compositions of human tissues by Woodard and White (1986)
  - 13 elements: H, C, N, O, Na, Mg, P, S, Cl, Ca, Fe, I
  - The 6 most important (> 0.6%) are H, C, N, O, P, Ca
  - Ex. of tissues with elemental fractional weights below

Tissue	ρ (g/cm^3)	H	C	N	O	Na	Mg	P	S	Cl	K	Ca	Fe	I
Lung deflated	0.260	0.103	0.105	0.031	0.749	0.002	0.000	0.002	0.003	0.003	0.002	0.000	0.000	0.000
Adipose tissue	0.950	0.114	0.598	0.007	0.278	0.001	0.000	0.000	0.001	0.001	0.000	0.000	0.000	0.000
Skeletal muscle	1.050	0.102	0.143	0.034	0.710	0.001	0.000	0.002	0.003	0.001	0.004	0.000	0.000	0.000
Liver	1.060	0.102	0.139	0.030	0.716	0.002	0.000	0.003	0.003	0.002	0.003	0.000	0.000	0.000
Thyroid	1.050	0.104	0.119	0.024	0.745	0.002	0.000	0.001	0.001	0.002	0.001	0.000	0.000	0.001
Sternum	1.250	0.078	0.316	0.037	0.438	0.000	0.001	0.040	0.002	0.001	0.001	0.085	0.001	0.000
Vert. col. whole	1.330	0.071	0.258	0.036	0.472	0.001	0.001	0.051	0.003	0.001	0.001	0.105	0.000	0.000
Ribs 2nd-6th	1.410	0.064	0.263	0.039	0.436	0.001	0.001	0.060	0.003	0.001	0.001	0.131	0.000	0.000
Ribs 10th	1.520	0.056	0.235	0.040	0.434	0.001	0.001	0.072	0.003	0.001	0.001	0.156	0.000	0.000
Sacrum male	1.290	0.074	0.302	0.037	0.438	0.000	0.001	0.045	0.002	0.001	0.001	0.098	0.001	0.000
Mandible	1.680	0.046	0.199	0.041	0.435	0.001	0.002	0.086	0.003	0.000	0.000	0.187	0.000	0.000
Cortical bone	1.920	0.034	0.155	0.042	0.435	0.001	0.002	0.103	0.003	0.000	0.000	0.225	0.000	0.000

- SP is directly proportional to electron density, thus and have direct impact on range
- *I*-values uncertainties can have an impact of up 1.1% on range (Bär *et al.*, PMB 2018)

Table 6. Calculated beam ranges in terms of R_{80} (in mm) using Monte Carlo proton beam transport simulations. The uncertainties reported are resulting from the uncertainties on our optimized I-values and the differences are taken between ranges simulated with ICRU-recommended I-values and ranges simulated with our optimized I-values.

Liquids and solids				
Material	Range ICRU	Range this work	Uncertainty (%)	Difference (%)
Water	202.25	203.35	0.95 (0.47%)	1.10 (0.54%)
Adipose tissue 3	211.97	212.72	0.79 (0.37%)	0.75 (0.35%)
Muscle skeletal 1	194.01	194.86	0.72 (0.37%)	0.85 (0.44%)
Brain white matter	194.68	195.55	0.72 (0.37%)	0.88 (0.45
Femur whole	151.49	152.34	0.47 (0.31%)	0.85 (0.56%)
Cortical bone	119.46	120.28	0.50 (0.42%)	0.82 (0.68%)

2. Principles of CT and role of X-ray energy on data

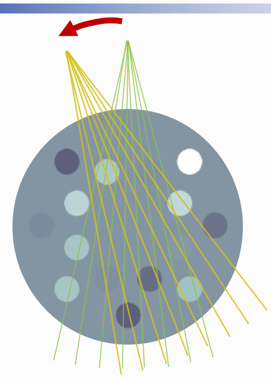

Tomographic scanning object

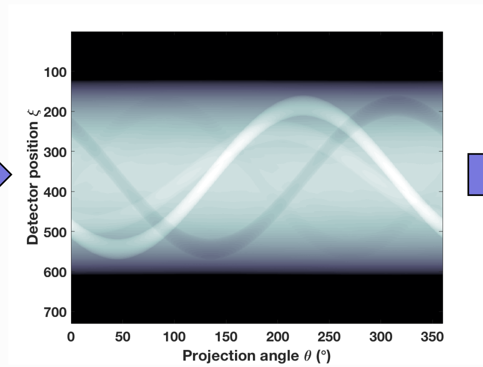

Monochromatic sinogram

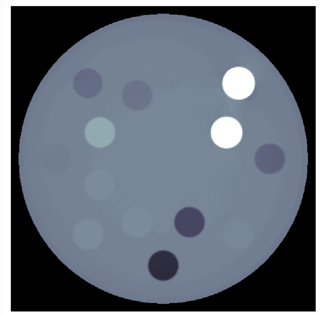

Reconstructed image

CT theory: the conversion of a 2D function into a sinogram representation is known as a *Radon transform* and its inverse operation often referred to as Filtered Back Projection

$$\mathscr{R}\left[f(x,y)\right]_{\xi,\gamma} = p(\xi,\gamma) = \int_{-\infty}^{\infty}\int_{-\infty}^{\infty} f(x,y)\,\delta(\xi - x\cos\gamma - y\sin\gamma)\,\mathrm{d}x\mathrm{d}y$$

$$\mathscr{R}^{-1}\left[p(\xi,\gamma)\right]_{x,y} = f(x,y) = \int_{0}^{\pi} \tilde{p}(x\cos\gamma + y\sin\gamma, \gamma)\,\mathrm{d}\gamma$$

with the filter $h(x) \equiv \mathscr{F}^{-1}\left[|k|\right]_x$ and the filtered projection $\tilde{p}(\xi,\gamma) \equiv \left[p(\xi,\gamma) * h(\xi)\right]_\xi$

- Typical CT reconstruction assumes monoenergetic scans. This causes an artefact called *beam hardening*, which results from the change in photon spectra as the X-ray travel through the object.

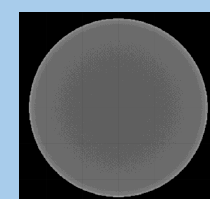

Example of BH artefact for a homogeneous cylindrical phantom

- Mathematically, the sinogram equation accounts for these spectral changes but it is impossible to resolve it exactly without spectral information.

$$T(\xi,\gamma) = \int_{0}^{h\nu_{\max}} \psi(h\nu)\, e^{-\mathscr{R}\left[\mu(x,y;h\nu)\right]_{\xi,\gamma}}\,\mathrm{d}h\nu$$
$$\approx e^{-\mathscr{R}\left[\tilde{\mu}(x,y)\right]_{\xi,\gamma}}$$

The sinogram equation and the monoener approximation to resolve an effective attenuation coefficient

2. Principles of CT and role of X-ray energy on data

- With ideal BH artefact correction algorithms, CT is an instrument to measure 3D distributions of X-ray attenuation coefficients

$$\frac{\mu}{\mu_{\mathrm{w}}} = \rho_{\mathrm{e}} \sum_i \lambda_i f\left(E, Z_i\right) \approx \rho_{\mathrm{e}} f\left(E, \tilde{Z}\right)$$

effective atomic number

μ_{W}: attenuation coefficient of water (cm^{-1})
$\boldsymbol{\rho}_e$: electron density relative to that of water
λ_i: electronic fraction of i^{th} element
f: electronic cross section relative to that of water and function of energy and Z

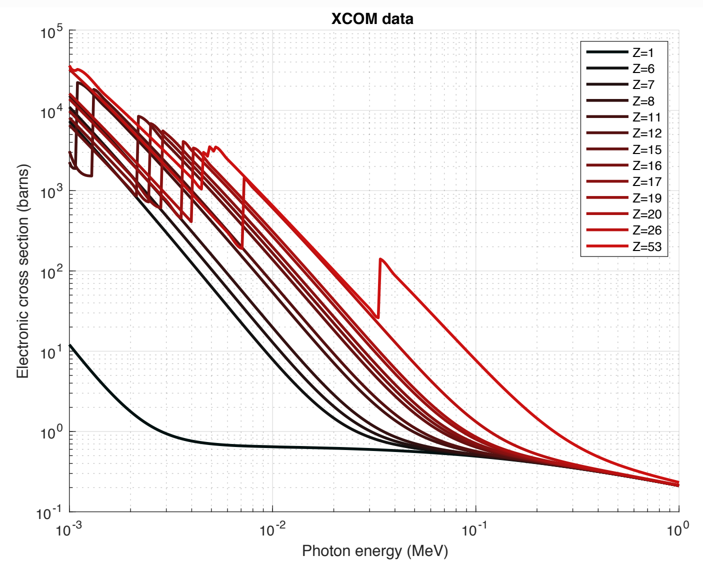

- For technical reasons, it is preferred to report the data in terms of units relative to water: Hounsfield unit

$$\mathrm{HU} = 1000\left[\frac{\mu}{\mu_{\mathrm{w}}} - 1\right]$$

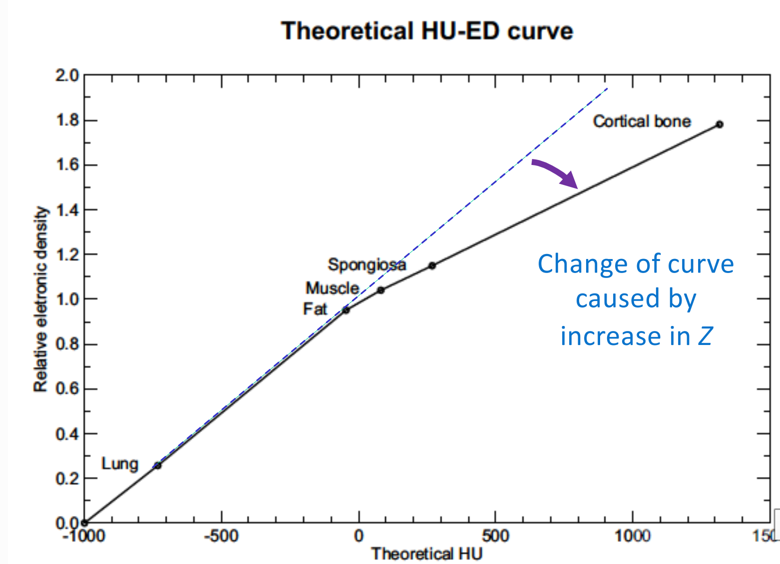

2. Principles of CT and role of X-ray energy on data

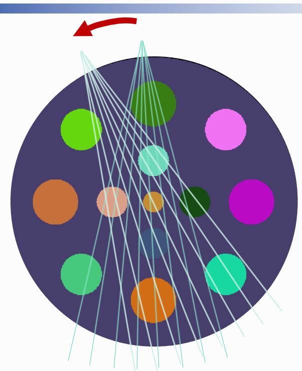

Colored tomographic scanning object

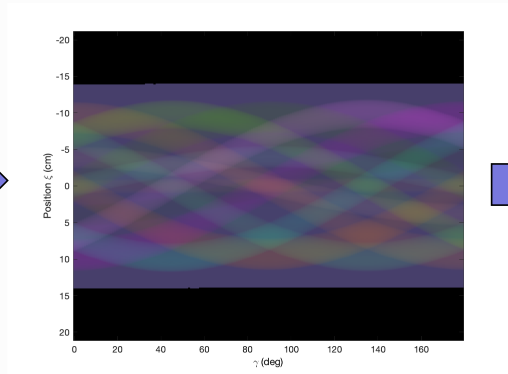

Polychromatic sinogram

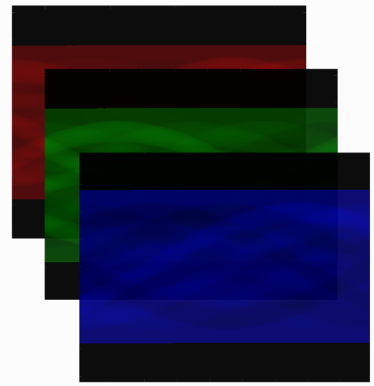

Decomposed monochromatic sinograms

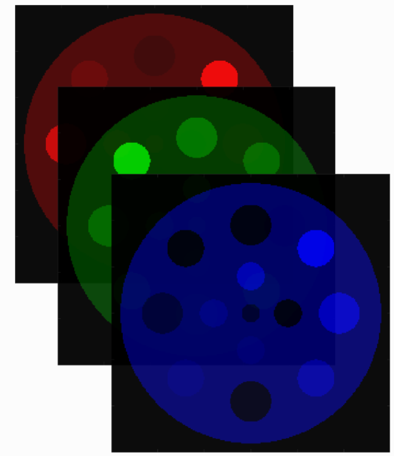

Reconstructed monochromatic images

Raw data-based approach

To treatment planning

Image-based approach

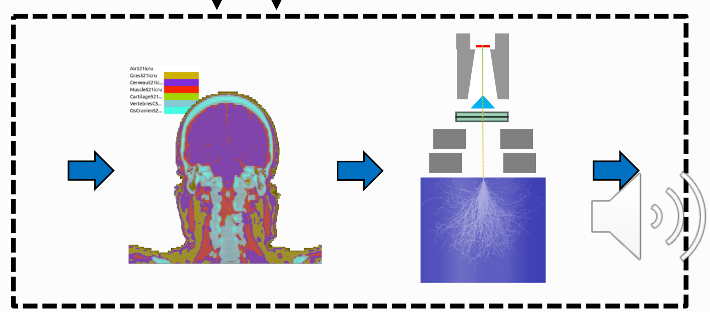

- Spectral CT opens the possibility to resolve information contained in CT data with more than 1 degree of freedom
  - Elemental composition and mass density
  - Parametric information resulting from elemental composition and mass density
- There are 2 ways to resolve information for RT
  - Image-based characterization direction on spectral HU
  - Resolving at the pre-reconstruction stage (raw data) to obtain sinograms of physical quantities

3. CT technologies for resolving energy

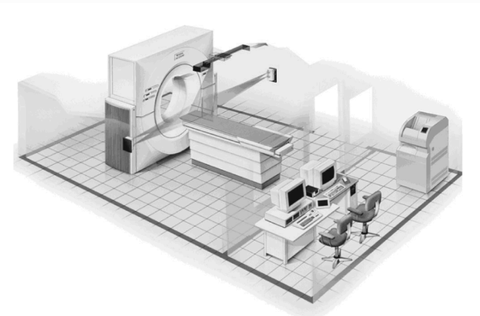

Mutic et al., Med Phys 2003

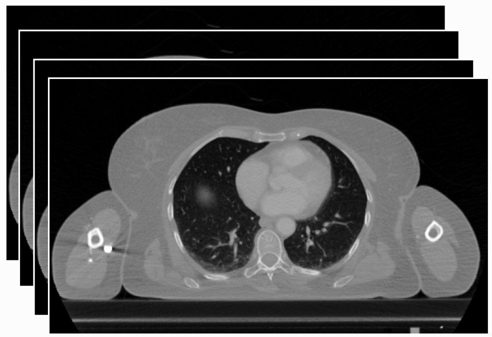

HU ambiguously specifies SPR: up to ~3% error

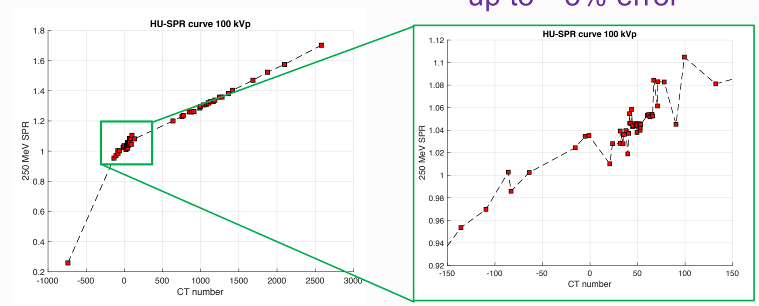

- For treatment planning we rely on CT's geometrical accuracy and speed of acquisition
- In conventional SECT, clinical dose calculation algorithms assign a single CT information per voxel
  - SPR lookup tables are used for semi-empirical dose calculation algorithms
  - Monte Carlo inputs require additional segmentation (Schneider *et al.,* PMB 2000)

In conventional SECT, we rely on natural correlations in human tissues

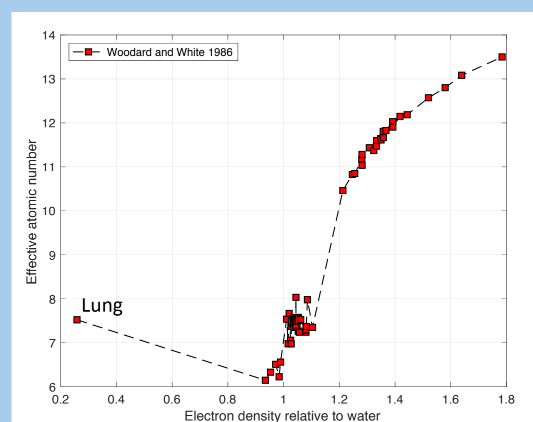

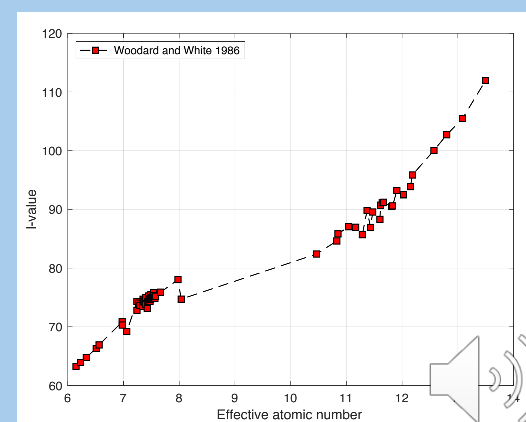

3. CT technologies for resolving energy

- Spectral CT offers a change of paradigm:
  - HU-SPR lookup tables are no longer needed
  - *N* independent information allows for solving *N* parameters

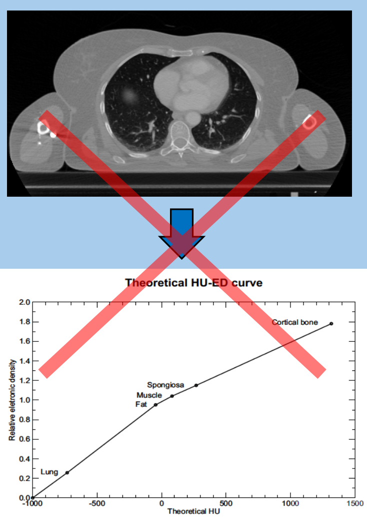

Spectral CT: principles of operation of some commercial scanners and other scanners under development

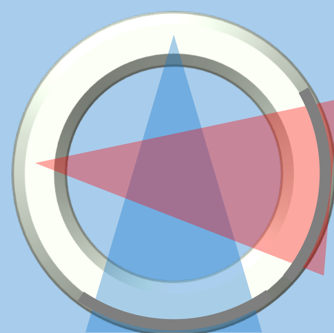

Dual-source CT (Siemens)

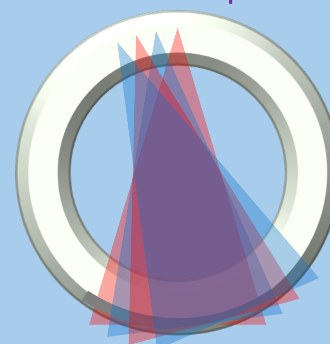

Rapid kV switchting (GE)

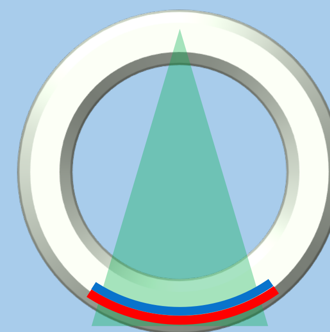

Dual-layer detector (Philips)

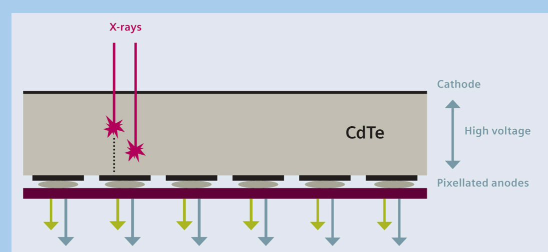

https://www.siemens-healthineers.com/

Siemens photon counting

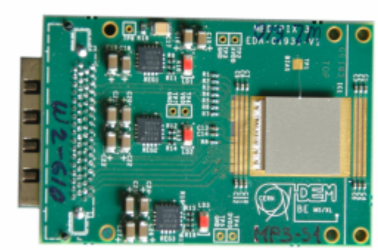

Ronaldson et al., JINST 2011

CERN's technologies (MARS)

3. CT technologies for resolving energy

Experimental measurements of SPR/range with animal tissue samples: improvements with DECT shown in 4 independent recent studies – the adapted approach of Schaffner and Pedroni, PMB 1998

Bär et al., Med Phys 2018

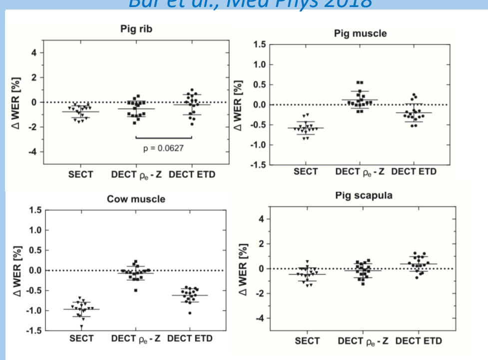

Möhler *et al., PMB* 2018

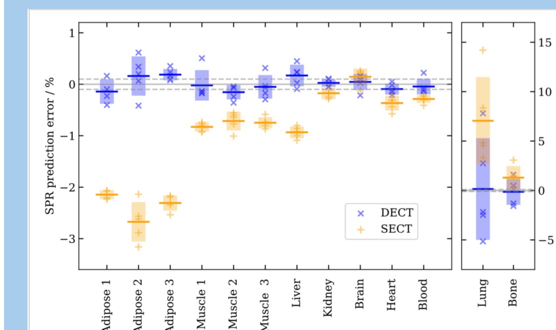

Xie *et al., PMB* 2018

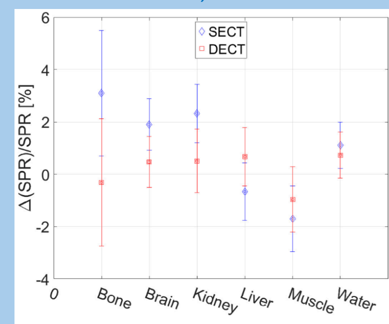

Taasti *et al.*, PMB 2017

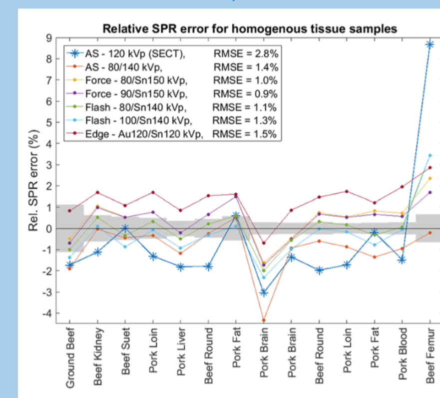

*Also quite a lot of work in literature to acknowledge on DECT: Bazalova *et al.* 2008; Yang *et al.* 2010, 2012; Landry *et al.* 2011, 2013a, 2013b; Hunemohr *et al.* 2014a, 2014b; Bourque *et al.* 2014; Han *et al.* 2016, 2017; Möhler *et al.*, 2016, Wohlfahrt *et al.* 2017; Berndt *et al.* 2017, Almeida *et al.* 2018;

Experimental measurements with MARS PCCT showed promise in gaining accuracy beyond 2 energies

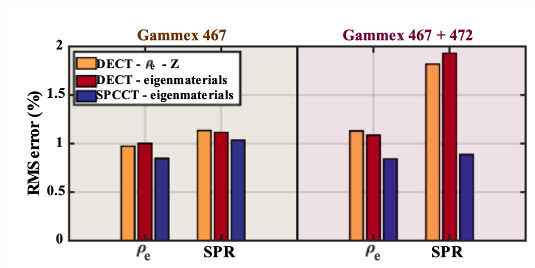

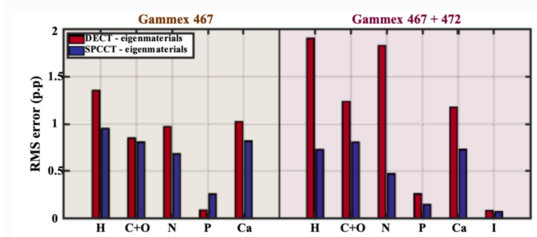

Simard *et al.*, Med Phys 2020

*Also quite a lot of work in literature to acknowledge on MECT: Lalonde & Bouchard 2016, Lalonde *et al.* 2017, Lalonde *et al.* 2018; Simard *et al.* 2019;

4. CT calibration for use in RT

- There exists 2 types of approaches (pre/post recon.) to spectral CT and several models for CT data
- All require a calibration phantom to resolve unknowns of the model to perform estimates
  - Use of calibration materials for which elemental composition are density is known
  - Solve coefficient with maximum likelihood

Original idea of CT calibration
(Schneider *et al.*, PMB 1996)

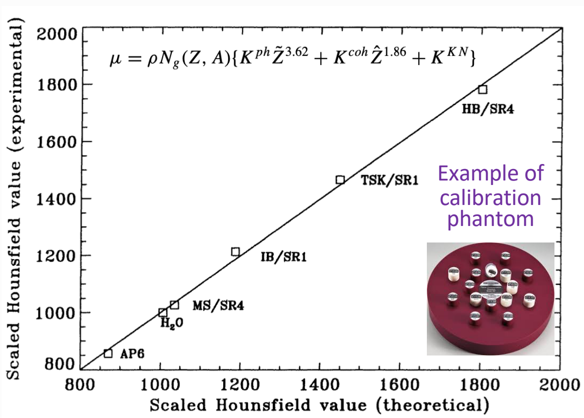

Various DECT theoretical models (Bär *et al.*, Med Phys 2017)

TABLE I. Summary of the theoretical foundation of different DECT formalisms.

	μ parametrization	Z definition	Requires CT calibration
Bazalova et al.	$\mu = \rho_e \sum_i w_i (Z^4 F(E_i, Z) + G(E_i, Z))$	Mayneord ($m = 3.5$)	No
Landry et al. #1 and #2	$\mu = \rho_e (A + BZ^m + CZ^n)$	Mayneord ($m = 3.3$)	Yes
Hünemohr et al. #1 and #2	$\mu = \rho_e (\alpha \frac{Z^m}{E^l} + \beta)$	Mayneord ($m = 3.1$)	Yes
Bourque et al.	$\mu/\mu_w = \rho_e \sum_{m=1}^{M} b_m Z^{m-1}$	Behavior of electronic cross sections for elements	Yes
Van Abbema et al.	$\mu = \int_0^\infty w(E)_e \sigma^{tot}(E, \widehat{Z}) dE$	Behavior of $\frac{\mu_L}{\mu_H}$ for mixtures	No
Han et al.	$\mu = c_1 \mu_1 + c_2 \mu_2$	None	Yes
Lalonde and Bouchard	$\mu/\mu_w = \bar{y}_0 f_0 + \sum_{k=1}^{K} y_k f_k$	None	Yes

4. CT calibration for use in RT

- Once you have a calibrated model, you can infer your material parameters from it
- Examples are
  - Electron density and effective atomic number
  - Fractional weights of base materials (e.g., eigentissues)
- The number of energies define the number of resolvable parameters: **number of energies ≥ number of parameters**

Material decomposition

$$\begin{pmatrix} u_1 \\ \vdots \\ u_N \end{pmatrix} = \begin{pmatrix} f_{11} & \cdots & f_{1N} \\ \vdots & \ddots & \vdots \\ f_{N1} & \cdots & f_{NN} \end{pmatrix} \begin{pmatrix} \xi_1 \\ \vdots \\ \xi_N \end{pmatrix}$$

Parametric model

$$\begin{aligned} u_1 &= f_1(\xi_1, \ldots, \xi_N) \\ &\vdots \\ u_N &= f_N(\xi_1, \ldots, \xi_N) \end{aligned}$$

The number of parameters ξ is typically equal to the number of energies N

Example of Schneider *et al*. 1996 applied to SECT and W&W data

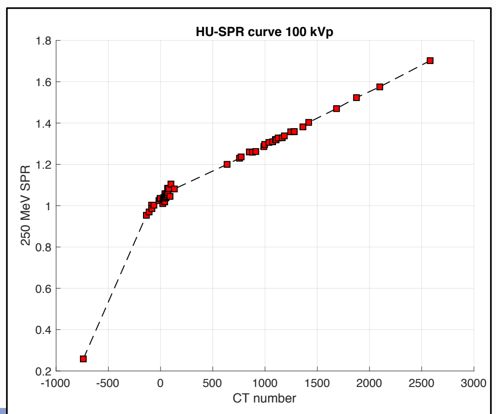

Various DECT formalisms models (Bär *et al*., Med Phys 2017)

TABLE II. Summary of different formalisms to predict tissue parameters with DECT.

	EAN	*I*-value	ED
Bazalova et al.	solve $\frac{u_L}{u_H}$ numerically	Yang et al.	substitute $\widehat{Z}$
Landry et al. #1 and #2	solve $\frac{u_L}{u_H}$ for Z	Yang et al. Bragg additivity rule	$\widehat{\rho}_e = \frac{\Delta HU}{1000} + 1$
Hünemohr et al. #1 and #2	substitute $\widehat{\rho}_e$	Yang et al. Bragg additivity rule	$\widehat{\rho}_e = \frac{1}{\beta} \frac{g_L \mu_H - g_H \mu_L}{g_L - g_H}$
Bourque et al.	$\widehat{Z}_{eff} = \sum_{k=1}^{K} c_k \Gamma^{k-1}$	5^{th}-order fit with Z_{med}	$\widehat{\rho}_{e,L/H} = \frac{u_{L/H}}{\sum_{m=1}^{M} b_{m,L/H} Z_{eff}^{m-1}}$
Van Abbema et al.	solve $\frac{\mu_L}{\mu_H}$ numerically	Yang et al.	substitute $\widehat{Z}$
Han et al.	None	$\widehat{I}_x = f_I\left(\frac{c_1}{c_1+c_2}\right) \exp\left(\frac{c_1 \rho_{e1} \ln(I_1) + c_2 \rho_{e2} \ln(I_2)}{c_1 \rho_{e1} + c_2 \rho_{e2}}\right)$	$\widehat{\rho}_{ex} = c_1 \rho_{e1} +$ [illegible] ρ_{e2}
Lalonde and Bouchard	None	Bragg additivity rule	$\widehat{\rho}_e = \bar{y}_0 +$ [illegible] y_x

4. CT calibration for use in RT

- Our ability to resolve a system of equation depends on its conditioning
- With linear systems, we use the *condition number* to evaluate the robustness of the system to its solution
- It is crucial to choose a model and a set of optimal scanning parameters that will yield the best condition number of your system

- Resolving multi-energy CT info involves the use of linear systems

$$\mathbf{y} = \mathbf{M}\mathbf{x} \Leftrightarrow \mathbf{x} = \mathbf{M}^{-1}\mathbf{y}$$

- The matrix $\mathbf{M}^{-1}$ acts as an "amplifier" on the measured **y**. The condition number of a matrix tells how experimental errors are amplified:

$$\frac{|\boldsymbol{\delta}\mathbf{x}|}{|\mathbf{x}|} \leq \kappa(\mathbf{M}) \frac{|\boldsymbol{\delta}\mathbf{y}|}{|\mathbf{y}|}$$

  - With the condition number defined as

$$\kappa(\mathbf{M}) \equiv ||\mathbf{M}||\,||\mathbf{M}^{-1}||$$

Dual-energy CT

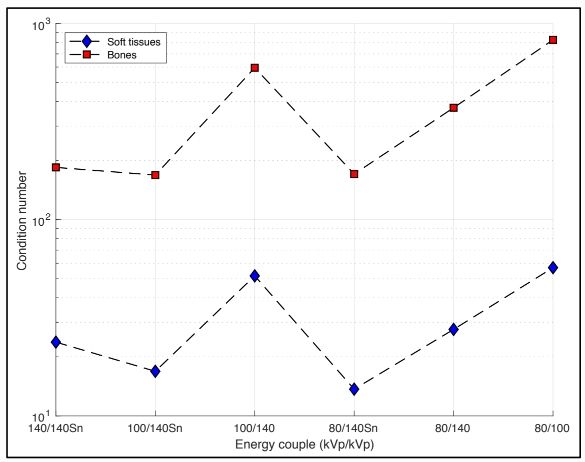

Multi-energy CT

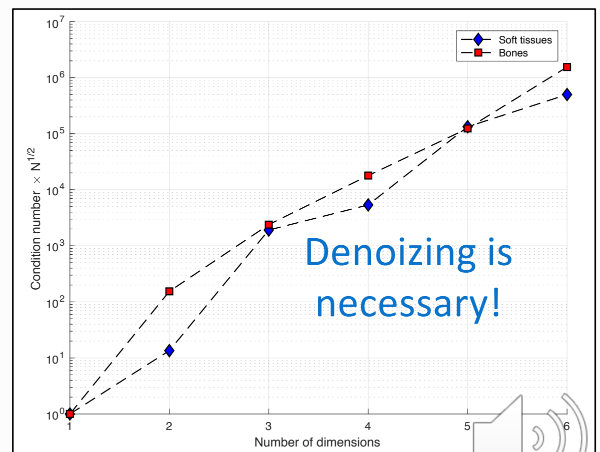

Denoizing is necessary!

5. Key radiotherapy quantities from CT

- All formalisms can yield “direct” estimations of electron density
- The ones with effective *Z* can yield an estimation of the *I*-value via additional fitting
- The parametric method benefits from natural correlations in human tissues

Yang *et al.*, PMB 2010

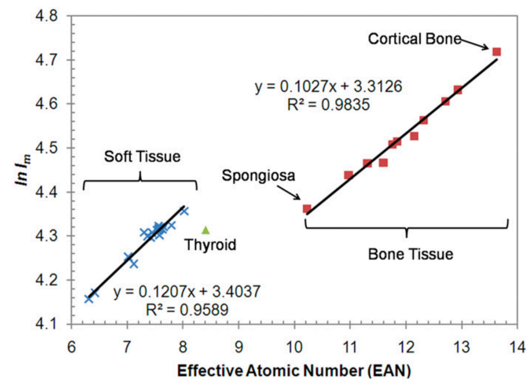

Figure 3. The soft tissue group and bony tissue group had separate linear relationships between the effective atomic number (EAN) and the logarithm of mean excitation energy (ln I_m) of the same tissue. Shown are plots for 34 standard human biological tissues listed in table 1.

Bourque *et al.*, PMB 2014

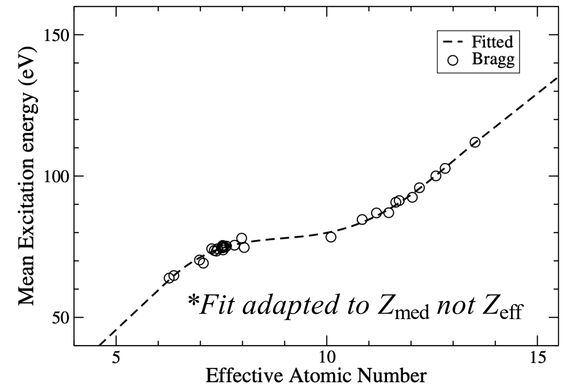

Figure 3. Parametrization of the ICRP mean excitation energy as a function of the EAN defined in this paper for human tissues.

- Some approaches can yield “direct” elemental composition and density estimations
  - Eigentissue decomposition (Lalonde and Bouchard, PMB 2016)
  - Parametric approach (Hünemohr et al., Med Phys 2014)

Example of eigentissue decomposition with a Siemens SOMATOM Definition Flash DSCT

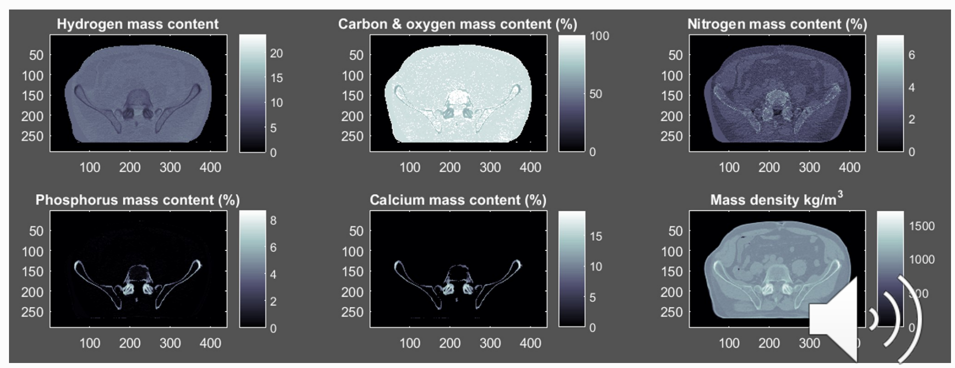

5. Key radiotherapy quantities from CT

- Contrast scans
  - The use of contrast agent can improve the localization of tumors
- Virtual non-contrast
  - Dual- and multi-energy CT enable to determine contrast agent concentrations and therefore produce non-contrast images by virtually removing the agent

- Many contrast agents
  - PCCT can manage several contrast agents in one scan

Lalonde et al., Med Phys 2019

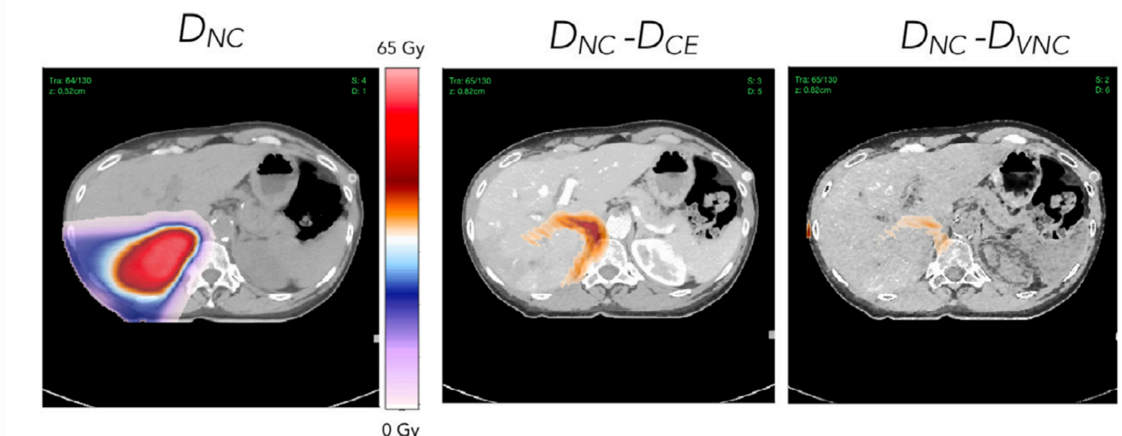

True non-contrast | Contrast-enhanced | Virtual non-contrast

Moghiseh *et al.*, JSM Biomed Im Data 2016.

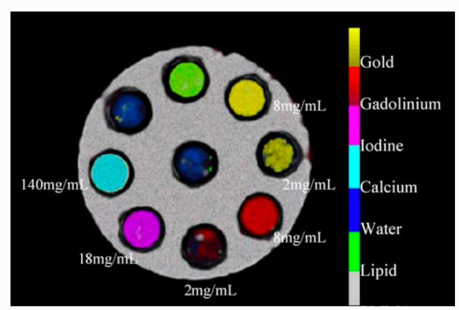

Cormode *et al.*, Scien Reports 2017

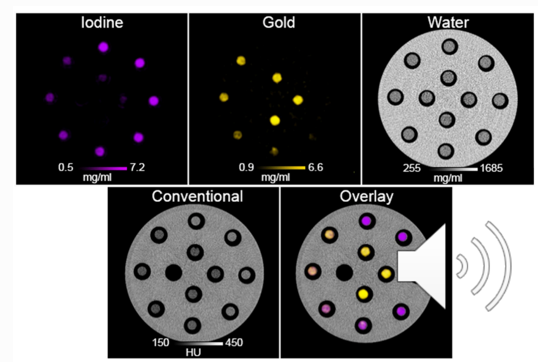

Take-home message: why spectral CT?

What we measure in CT:
how photons interact

The connection:
elemental composition and density

What we need for RT:
how p+ beams interact

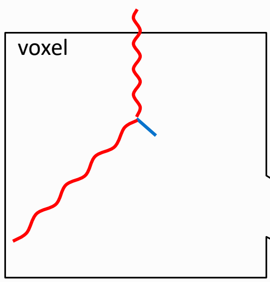

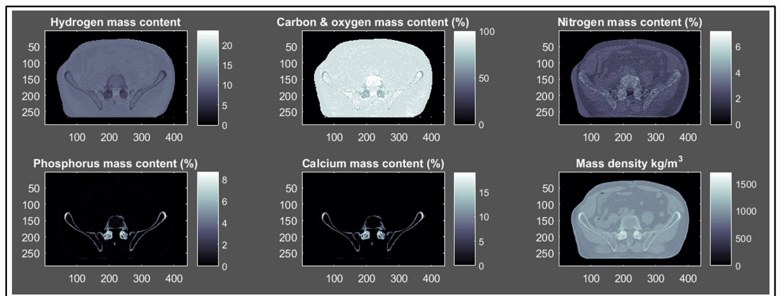

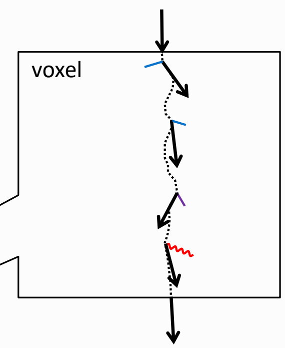

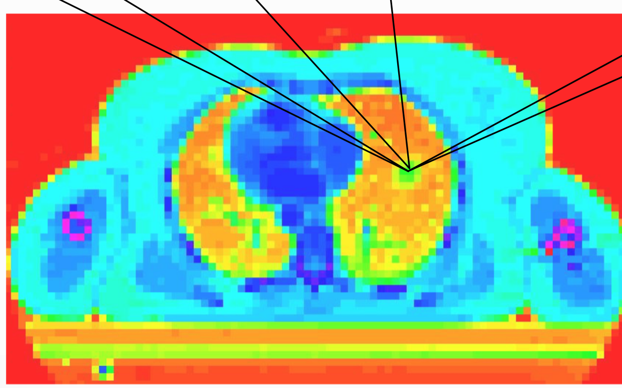

Questions?

"He must be very ignorant for he answers every question he is asked"
\- Voltaire.

Selected reference (there are many others mentioned in this presentation and in literature!)

- Schneider, U., Pedroni, E. and Lomax, A., 1996. The calibration of CT Hounsfield units for radiotherapy treatment planning. Physics in Medicine & Biology, 41(1), p.111.
- Schneider, W., Bortfeld, T. and Schlegel, W., 2000. Correlation between CT numbers and tissue parameters needed for Monte Carlo simulations of clinical dose distributions. *Physics in Medicine & Biology*, *45*(2), p.459.
- Williamson, J.F., Li, S., Devic, S., Whiting, B.R. and Lerma, F.A., 2006. On two-parameter models of photon cross sections: Application to dual-energy CT imaging. Medical physics, 33(11), pp.4115-4129.
- Flohr, T.G., McCollough, C.H., Bruder, H., Petersilka, M., Gruber, K., Süβ, C., Grasruck, M., Stierstorfer, K., Krauss, B., Raupach, R. and Primak, A.N., 2006. First performance evaluation of a dual-source CT (DSCT) system. European radiology, 16(2), pp.256-268.
- Schlomka, J., Roessl, E., Dorscheid, R., Dill, S., Martens, G., Istel, T., Bäumer, C., Herrmann, C., Steadman, R., Zeitler, G. and Livne, A., 2008. Experimental feasibility of multi-energy photon-counting K-edge imaging in pre-clinical computed tomography. Physics in Medicine & Biology, 53(15), p.4031.
- Bazalova, M., Carrier, J.F., Beaulieu, L. and Verhaegen, F., 2008. Dual-energy CT-based material extraction for tissue segmentation in Monte Carlo dose calculations. *Physics in Medicine & Biology*, *53*(9), p.2439.
- Yang, M., Virshup, G., Clayton, J., Zhu, X.R., Mohan, R. and Dong, L., 2010. Theoretical variance analysis of single-and dual-energy computed tomography methods for calculating proton stopping power ratios of biological tissues. Physics in Medicine & Biology, 55(5), p.1343.
- Saito, M., 2012. Potential of dual-energy subtraction for converting CT numbers to electron density based on a single linear relationship. Medical physics, 39(4), pp.2021-2030.
- Landry, G., Seco, J., Gaudreault, M. and Verhaegen, F., 2013. Deriving effective atomic numbers from DECT based on a parameterization of the ratio of high and low linear attenuation coefficients. Physics in Medicine & Biology, 58(19), p.6851.
- Bourque, A.E., Carrier, J.F. and Bouchard, H., 2014. A stoichiometric calibration method for dual energy computed tomography. Physics in Medicine & Biology, 59(8), p.2059.
- Hünemohr, N., Paganetti, H., Greilich, S., Jäkel, O. and Seco, J., 2014. Tissue decomposition from dual energy CT data for MC based dose calculation in particle therapy. Medical physics, 41(6Part1), p.061714.
- Lalonde, A. and Bouchard, H., 2016. A general method to derive tissue parameters for Monte Carlo dose calculation with multi-energy CT. Physics in Medicine & Biology, 61(22), p.8044.
- van Elmpt, W., Landry, G., Das, M. and Verhaegen, F., 2016. Dual energy CT in radiotherapy: current applications and future outlook. Radiotherapy and Oncology, 119(1), pp.137-144.
- Lalonde, A., Bär, E. and Bouchard, H., 2017. A Bayesian approach to solve proton stopping powers from noisy multi-energy CT data. Medical physics, 44(10), pp.5293-5302.
- Bär, E., Lalonde, A., Royle, G., Lu, H.M. and Bouchard, H., 2017. The potential of dual-energy CT to reduce proton beam range uncertainties. Medical physics, 44(6), pp.2332-2344.
- Panta, R.K., Butler, A.P., Butler, P.H., de Ruiter, N.J., Bell, S.T., Walsh, M.F., Doesburg, R.M., Chernoglazov, A.I., Goulter, B.P., Carbonez, P. and Damet, J., 2018, November. First human imaging with MARS photon-counting CT. In 2018 IEEE Nuclear Science Symposium and Medical Imaging Conference Proceedings (NSS/MIC) (pp. 1-7). IEEE.